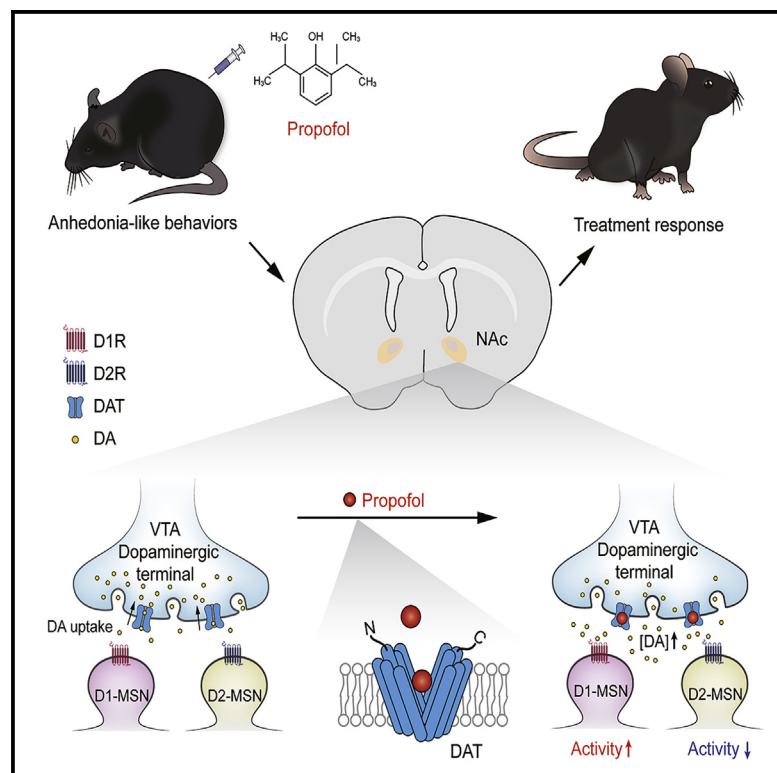


Propofol exerts anti-anhedonia effects via inhibiting the dopamine transporter

Graphical abstract



Authors

Xiao-Na Zhu, Jie Li, Gao-Lin Qiu, ..., Tao Xu, Ti-Fei Yuan, Ji Hu

Correspondence

balor@sjtu.edu.cn (T.X.),
tifei.yuan@smhc.org.cn (T.-F.Y.),
huji@shanghaitech.edu.cn (J.H.)

In brief

Zhu et al. discover that propofol inhibits the dopamine transporter (DAT) and rapidly enhances the dopamine concentration in the NAc, which relieves stress-induced anhedonia.

Highlights

- Propofol directly binds to and inhibits the dopamine transporter (DAT)
- Propofol elevates dopamine concentration in the nucleus accumbens (NAc)
- Propofol induces the potentiation of NAc D1-MSNs
- Propofol rapidly reverses anhedonia in which the potentiation of D1-MSNs is necessary

Article

Propofol exerts anti-anhedonia effects via inhibiting the dopamine transporter

Xiao-Na Zhu,^{1,5} Jie Li,^{2,5} Gao-Lin Qiu,^{3,5} Lin Wang,¹ Chen Lu,¹ Yi-Ge Guo,¹ Ke-Xin Yang,¹ Fang Cai,¹ Tao Xu,^{4,*} Ti-Fei Yuan,^{2,*} and Ji Hu^{1,6,*}

¹School of Life Science and Technology, ShanghaiTech University, Shanghai 201210, China

²Shanghai Key Laboratory of Psychotic Disorders, Brain Health Institute, National Center for Mental Disorders, Shanghai Mental Health Center, Shanghai Jiao Tong University School of Medicine, Shanghai 200030, China

³Department of Anesthesiology, First Affiliated Hospital of Anhui Medical University, Hefei 230022, China

⁴Department of Anesthesiology, Affiliated Shanghai Sixth People's Hospital, Shanghai Jiao Tong University School of Medicine, Shanghai 200233, China

⁵These authors contributed equally

⁶Lead contact

*Correspondence: balor@sjtu.edu.cn (T.X.), tifei.yuan@smhc.org.cn (T.-F.Y.), huji@shanghaitech.edu.cn (J.H.)
<https://doi.org/10.1016/j.neuron.2023.02.017>

SUMMARY

Lasker's award-winning drug propofol is widely used in general anesthesia. The recreational use of propofol is reported to produce a well-rested feeling and euphoric state; yet, the neural mechanisms underlying such pleasant effects remain unelucidated. Here, we report that propofol actively and directly binds to the dopamine transporter (DAT), but not the serotonin transporter (SERT), which contributes to the rapid relief of anhedonia. Then, we predict the binding mode of propofol by molecular docking and mutation of critical binding residues on the DAT. Fiber photometry recording on awake freely moving mice and [¹⁸F] FP-CIT-PET scanning further establishes that propofol administration evokes rapid and lasting dopamine accumulation in nucleus accumbens (NAc). The enhanced dopaminergic tone drives biased activation of dopamine-receptor-1-expressing medium spiny neurons (D1-MSNs) in NAc and reverses anhedonia in chronically stressed animals. Collectively, these findings suggest the therapeutic potential of propofol against anhedonia, which warrants future clinical investigations.

INTRODUCTION

Anhedonia, the loss of interest or pleasure in usual activities, is prevalent in modern society and increased tremendously during the COVID-19 pandemic.¹ It is one of the core symptoms for several major psychiatric disorders, especially major depressive disorder (MDD).² Anhedonia predicts for poor long-term outcomes, such as suicide and non-response to drug treatments.³ In clinical practice, there is currently a lack of effective and rapidly acting therapies against anhedonia, largely due to insufficient understanding of the underlying neural mechanisms. Previous studies indicated that the nucleus accumbens (NAc) plays a critical role in regulating hedonic status through local dopaminergic signaling.^{4,5} Specifically, such regulation is implemented via balanced activities of medium spiny neurons (MSNs) expressing dopamine receptor 1 (D1R) and dopamine receptor 2 (D2R),⁶ which exhibit differential and often opposing roles in motivation and reinforcement.^{5,7} Modulating accumbal dopaminergic tone, therefore, may rebalance the valence coding for pleasure and treat anhedonia.

The recreational use of anesthetic agents such as diethyl ether, ketamine, propofol, and laughing gas has more than 150

years of history. The intravenous administration of propofol generates euphoric moods and lasting relaxation.⁸ A pilot study using microdialysis reported that propofol could elevate dopamine concentration in the NAc,⁹ yet its molecular targets and circuit mechanism remain unclear. This phenomenon could hardly be explained by its classical role as a GABA_AR agonist that silences midbrain dopamine neurons. One plausible hypothesis is that propofol may interrogate the dopamine reuptake machinery after terminal release. In addition, the potential effects of propofol on anhedonia have not been systemically investigated.

Dopamine transporter (DAT) acts as a key arbiter in regulating extracellular dopamine homeostasis, which has also been proposed as the core mechanism underlying the addictive potential of cocaine. DAT mutation is associated with increased risk of Parkinson's disease, attention deficit hyperactivity disorder (ADHD), and depression.^{10,11} Moreover, genetic ablation of DAT in rats results in motor hyperactivity, compulsive-like traits, and hedonism. It is conceivable that propofol could interact with DAT to regulate dopaminergic signaling in the NAc.

We here combine molecular, structural, and neurobiological approaches to uncover propofol's previously undetermined molecular target in pursuit of a novel therapeutic application. We

first employed molecular docking and mutation-based assays to reveal the potential binding sites and molecular mechanism of propofol on DAT, in comparison with the classical binding sites of dopamine. We then used fiber photometry recording on freely moving animals and positron emission tomography (PET) imaging to measure the effects of propofol on dopaminergic signaling in the NAc *in vivo*. We further examined the behavioral effects of propofol administration on anhedonic status in a mouse model of chronic restraint stress (CRS), and we manipulated D1 receptor signaling and activity of D1-MSNs to dissect the potential neural mechanisms. These results validate the therapeutic potential of targeting DAT for anhedonia treatment and may support the non-anesthetic use of propofol in psychiatric diseases.

RESULTS

Propofol inhibits dopamine transport by binding to DAT

We first employed filtration-based radioligand binding and [^3H]-DA uptake assays to determine the inhibition of DAT by propofol *in vitro*. Propofol significantly inhibited DAT but not the serotonin transporter (SERT) (Figures 1A–1D). To achieve insight into the molecular basis for the inhibition of propofol to DAT, we performed homology modeling and molecular docking to acquire the binding mode of dopamine and propofol. The results indicated that propofol occupied the transport channel of DAT rather than directly competing with dopamine (Figure 1E). Based on the predicted binding mode (Figure 1F) and protein-ligand interaction contacts in the molecular dynamics (MDs) (Figure S1A) of dopamine and propofol with DAT, we performed a mutation-based assay to assess propofol's functional binding to DAT. First, we designed the F76A, D79A, V152A, Y156F, and F325A mutants to verify the DAT-dopamine-binding mode. Among these mutants, the F76A, V152A, and F325A could reduce hydrophobic complementarity between DAT and dopamine, the D79A could break the salt bridge between D79 with the amino of dopamine, and the Y156F could destabilize the conformation of D79 and the salt bridge between D79 with dopamine. To detect the transport activity of DAT, we quantified the uptake of a fluorescent substrate of DAT, 4-(4-dimethylamino-2-ethyl)-N-methylpyridinium (ASP+), via live cell confocal microscopy in GFP-DAT cells at millisecond time resolution.¹² In line with predictions, all the designed mutations are capable of blocking the transport function of DAT in the functional assay, but none of them affect the expression of DAT (Figures 1G, 1H, S1B, and S1C). After that, we also selected three residues far from the dopamine-binding pocket to verify the binding mode of propofol. The A81F was designed to promote steric clashes and block the propofol-binding pocket, the F155Y broke the pi-pi stacking with the benzene ring of propofol, and the D475A broke the hydrogen bond with the hydroxyl group of propofol. All these mutants were demonstrated by DAT functional assay to block the inhibitory effect of propofol (Figures 1I and S1D; Table S1) and did not affect the transport function of DAT (Figure 1H). These findings support our hypothesis that propofol inhibits DAT transport activity by blocking the channel rather than competitively binding to dopamine.

Furthermore, we found that the 2,4-di-tert-butylphenol, a propofol analog, could inhibit DAT, but the other analogs¹⁴ are inactive

for DAT (Figure S2A). Based on the binding site of propofol, we found that the docking score and molecular mechanics Poisson-Boltzmann surface area (MM/GBSA) binding free energy could significantly discriminate between active and inactive compounds of DAT (Figure S2B; Table S2). These results were consistent with the molecular docking, which indicated that propofol docks a novel ligand-binding pocket to block the DAT function.

Propofol enhances NAc dopamine levels *in vivo*

To probe the potency of propofol's effect on the dopaminergic system *in vivo*, we performed [^{18}F] FP-CIT (a particular DAT ligand) based PET scanning on mice. Propofol efficiently reduced DAT availability in the striatum, suggesting that propofol could bind to DAT and elevate the dopamine concentration in the NAc (Figures 2A–2C). Next, we performed continuous recording to monitor *in vivo* dopamine dynamics with fiber photometry, using a genetically encoded dopamine probe (AAV-hsyn-DA1m-WPRE-PA)¹⁵ or serotonin probe (AAV-hSyn-5HT1.0-WPRE-PA)¹⁶ in NAc (Figures 2D and S10A). A stable DA1m signal baseline was first established before the injection of saline or propofol (25, 50, 75, or 100 mg/kg). Propofol at 100 mg/kg significantly increased dopamine but not serotonin levels in the NAc (Figures 2E and 2F), an effect which could be blocked by GBR12909, a highly selective antagonist of DAT (Figure 2G). To exclude the direct binding effect of propofol on the DA-1m sensor and fluorescence intensity, we conducted *in vitro* experiments and found that the DA-1m sensor exhibited robust fluorescence enhancement to DA, which could be blocked by the co-application of D2R antagonist haloperidol (Halo). However, propofol application did not result in a direct DA1m fluorescence increase (Figure S3).

A previous study reported that propofol could activate ventral tegmental area (VTA) dopamine neurons and increase dopamine concentration.¹⁷ We therefore recorded calcium activity on VTA dopamine neurons, the primary source of dopaminergic projection to the NAc. We injected Cre-dependent AAV-EF1 α -DIO-GCaMP6m virus into the VTA of DAT-ires-Cre mice (Figures S4A and S10B) and found that propofol administration decreased VTA DA neuron activities in control and CRS mice (Figures S4B–S4E, S4I, and S4J). In the brain slice electrophysiology recording, propofol also inhibited the activity of DA neuron in the VTA, and such suppressive effects were blocked by GABA_A receptor antagonist (picrotoxin 50 μM) (Figures S4F and S4K), but not by D2R antagonist (sulpiride 50 μM) (Figures S4G and S4L). However, in the presence of a D2R antagonist, the degree of VTA DA neurons inhibition by propofol was weakened, suggesting the potential involvement of D2R in mediating propofol's inhibition of VTA DA neurons (Figure S4H). These data indicate that propofol inhibits VTA dopamine neurons.

Propofol regulates the activity of NAc MSNs in control and CRS mice

In the NAc, D1- and D2-MSNs are the downstream responders for dopaminergic signaling and contribute to potentially distinct aspects of reward processing.¹⁸ We first examined propofol's effects on these two populations of neurons using *in vitro* brain slice electrophysiology recording in control and CRS mice. In

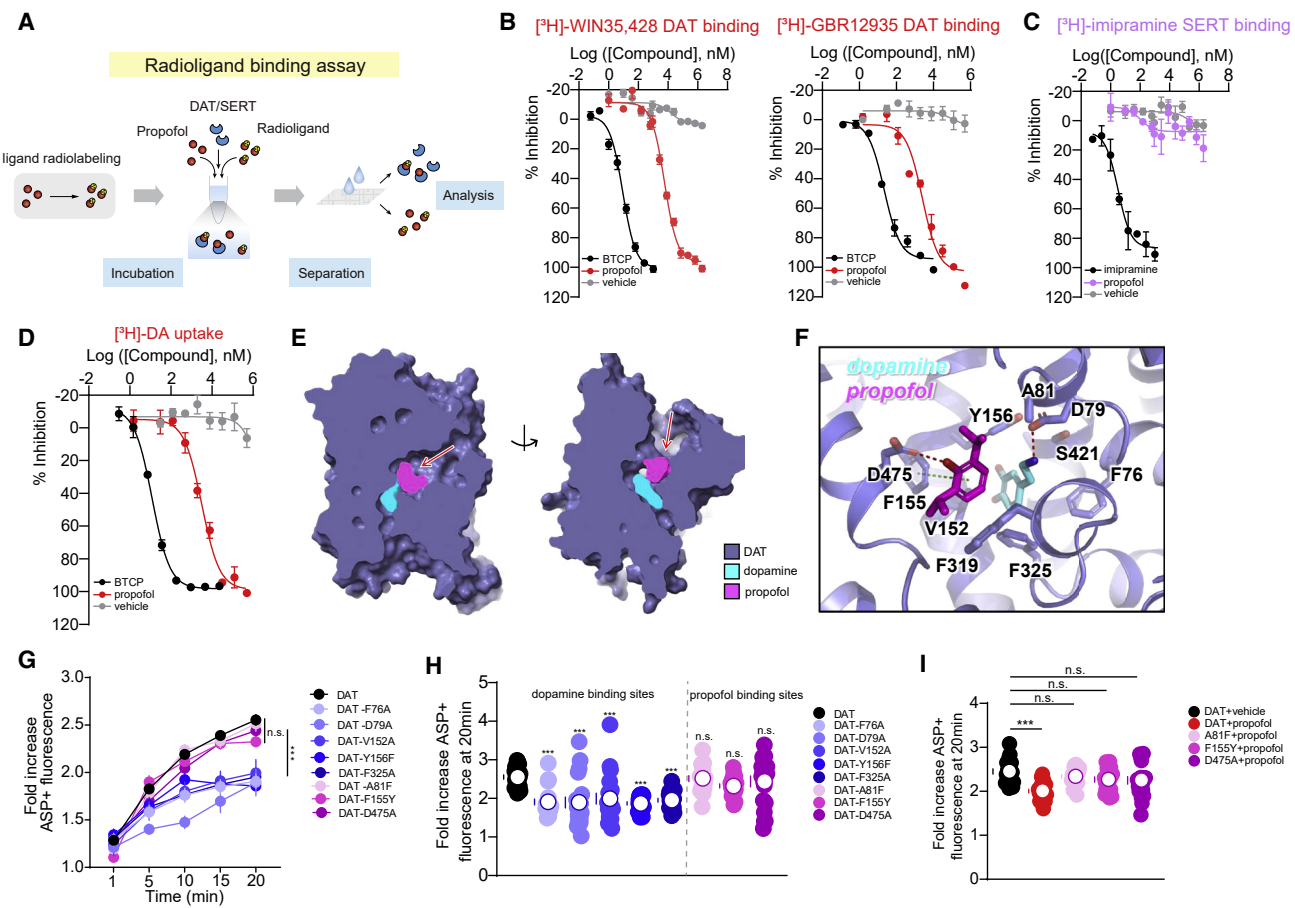


Figure 1. Propofol inhibits dopamine transport by binding to DAT

(A) The experimental process of a radioligand-binding assay combining propofol with DAT or SERT.

(B) Representative curves of the dose-dependent inhibition of [3 H]-WIN35,428 and [3 H]-GBR12935 binding by propofol to DAT. BTCP was used as a positive control. Estimated K_i value of propofol and DAT is 3.41 μ M ([3 H]-WIN35,428) (BTCP, K_i = 5.27 nM; L = 12.5 nM, K_d = 18 nM), and 1.14 μ M ([3 H]-GBR12935) (BTCP, K_i = 10.00 nM; L = 2 nM, K_d = 1.68 nM).

(C) Representative curves of the dose-dependent inhibition of [3 H]-imipramine binding by propofol to SERT. Imipramine was used as a positive control. (imipramine, K_i = 1.75 nM; L = 2 nM, K_d = 2.4 nM) (n = 4 independent experiments).

(D) Representative curves of the dose-dependent inhibition of [3 H]-DA uptake by propofol to DAT. Estimated K_i value of propofol and DAT is 3.13 μ M (BTCP, K_i = 10.38 nM; L = 10 nM, K_m = 580 nM 13) (n = 4 independent experiments).

(E) The binding sites of dopamine and propofol in the transport channel of DAT, the pocket occupied by propofol is indicated by a red arrow.

(F) The binding mode of propofol and dopamine. The hydrogen bonds are shown in the red dashed line and the pi-pi stacking is shown in the green dashed line.

(G and H) The mutants in dopamine-binding sites (DAT-F76A, DAT-D79A, DAT-V152A, DAT-Y156F, and DAT-F325A) significantly decreased ASP+ uptake compared with DAT, while the mutants in propofol-binding sites (DAT-A81F, DAT-F155Y, and DAT-D475A) did not affect ASP+ uptake (n = 20) during the course of 20 min (G). (H) Fold ASP+ fluorescence during 20 min as in (G).

(I) DAT + propofol (n = 20) significantly decreased ASP+ uptake compared with DAT (n = 20), while DAT-A81F + propofol, DAT-F155Y + propofol, and DAT-D475A + propofol did not affect ASP+ uptake (n = 20) during the 20 min (n represents independent cells). Statistical significance was determined by two-way ANOVA followed by Dunnett's multiple comparisons test (G) and one-way ANOVA followed by Dunnett's multiple comparisons test (H and I). Data are presented as the mean \pm SEM. *** p < 0.001.

See also [Figures S1 and S2](#) and [Tables S1 and S2](#).

CRS mice, the D1-MSNs showed reduced neuronal excitability, which was reversed by the perfusion of propofol (10 μ M) ([Figures 3A–3C](#)). On the other hand, D2-MSNs in CRS mice also exhibited reduced excitability when compared with control animals, while propofol induced further inhibition of the neuronal firing ([Figures 3E–3G](#)). The DAT inhibitor, GBR12909, blocked the effect of propofol on the excitability of both D1-MSNs and D2-MSNs ([Figures 3D and 3H](#)).

We then injected Cre-dependent AAV-EF1 α -DIO-GCaMP6m virus into the NAc of D1-Cre and D2-cre mice ([Figures 3I, S10C, and S10D](#)) and used fiber photometry to record changes in the Ca $^{2+}$ signals of the two neuronal populations *in vivo*. As demonstrated on brain slices, D1-MSNs showed enhanced activity while D2-MSNs' activity was suppressed on a comparable timescale (e.g., more than 1 h) in control and CRS mice ([Figures 3J and 3K](#)). We also employed the AAV

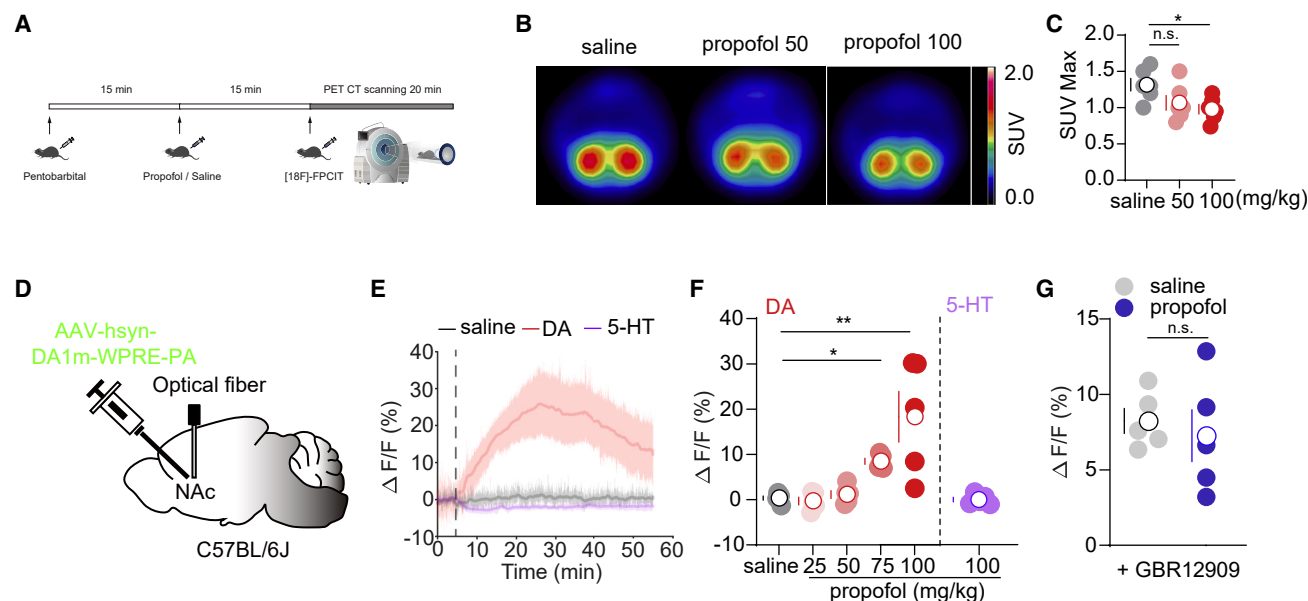


Figure 2. Propofol enhances NAc dopamine levels *in vivo*

(A) Treatment protocol for measuring changes of DAT availability using PET scanning.

(B) [^{18}F]-FPCIT PET brain image co-registered to a computed tomography (CT) scan demonstrating high signal-to-noise ratio in striatal uptake from representative mice treated with saline or propofol and showing decreased uptake in propofol-treated mice. Standardized uptake value (SUV) is presented as summed activity at the 20 min used to measure the DAT availability.

(C) Quantification of SUV max in saline and propofol (50 and 100 mg/kg) groups ($n = 6$ mice per group). PET, positron emission tomography; CT, computed tomography.

(D) Schematic of virus injection to express DA-1m in NAc with the optical fiber implanted above NAc.

(E) DA-1m and 5-HT sensor signals from NAc aligned to the moment of the administration of saline and propofol (100 mg/kg). Mean values are shown as a red line (DA-1m), a gray line (saline), and a purple line (5-HT sensor), SEM, interval is shaded in red, gray, and purple.

(F) Quantification of change in DA-1m and 5-HT sensor signals after administration of saline and propofol (25, 50, 75, and 100 mg/kg) ($n = 5$ mice per group).

(G) Quantification of change in DA-1m signals after administration of saline and propofol (100 mg/kg) after pre-administration of GBR12909 (10 mg/kg) ($n = 5$ mice per group). DA-1m, a G-protein-coupled, receptor-activation-based dopamine sensor; 5-HT sensor, a G-protein-coupled, receptor-activation-based serotonin sensor. Statistical significance was determined by one-way ANOVA followed by Dunnett's multiple comparisons test (C and F) and unpaired Student's *t* test. (G) Data are presented as the mean \pm SEM. * $p < 0.05$; ** $p < 0.01$.

See also [Figures S3](#) and [S10](#).

shRNA knockdown strategy to reduce the DAT expression, then conducted photometry recording and *in vitro* brain slice electrophysiology recording. The results showed that knocking down DAT could abolish the effect of propofol on both dopamine levels and the activation of D1-MSNs ([Figure S5](#)).

Propofol reverses anhedonia in CRS mice

Patients with propofol anesthesia may experience euphoria.^{8,19} We further investigated the potential hedonic responses to different doses of propofol (25, 50, and 100 mg/kg) using a mouse model of CRS (16 days). A single propofol exposure at 100 mg/kg (but not 25 or 50 mg/kg) could rapidly and selectively reverse anhedonic behavior 4 h after administration, but did not improve helplessness behavior (e.g., tail suspension test [TST], forced swimming test [FST]) ([Figures 4A–4D](#)) or anxiety-like behavior ([Figure S6](#)) in CRS mice. Repeated exposure to propofol (100 mg/kg) for 5 consecutive days revealed similar results ([Figures S7A–S7D](#)). In addition, a single dose of propofol could have long-lasting effects on anhedonic behavior after 24 h and 3 days, but did not have such effects on helplessness behaviors (e.g., TST, FST) ([Figures 4E–4J](#) and [S7E–S7P](#)). To exclude the potential confound-

ing effects of sedation on the behavioral measurements, we determined that the administration of pentobarbital at a sedative dosage did not affect anhedonia ([Figures 4E–4J](#)).

We then examined action potentials (APs) and spontaneous excitatory postsynaptic currents (sEPSCs) from NAc D1-MSNs. We observed that the intrinsic excitability and the frequency of sEPSCs were increased in the propofol treatment group 4 h after injection ([Figure S8](#)), indicating that the activated D1-MSNs 4 h after propofol treatment may be involved in regulating anhedonia-like behavior. Notably, control and stressed mice receiving propofol (40 or 100 mg/kg) for 7 days showed no conditional place preference (CPP) formation, unlike mice receiving GBR12909 (10 mg/kg), cocaine (15 mg/kg), or morphine (15 mg/kg) ([Figures 4K, 4L, and S9](#)), indicating that the addiction risks with this dosage and exposure scheme are limited.

Propofol rapidly attenuates anhedonia through NAc D1-MSNs activation

Since propofol is a robust GABA_A receptor agonist, we performed local application of SCH23390 (D1 receptor inhibitor) or PTX

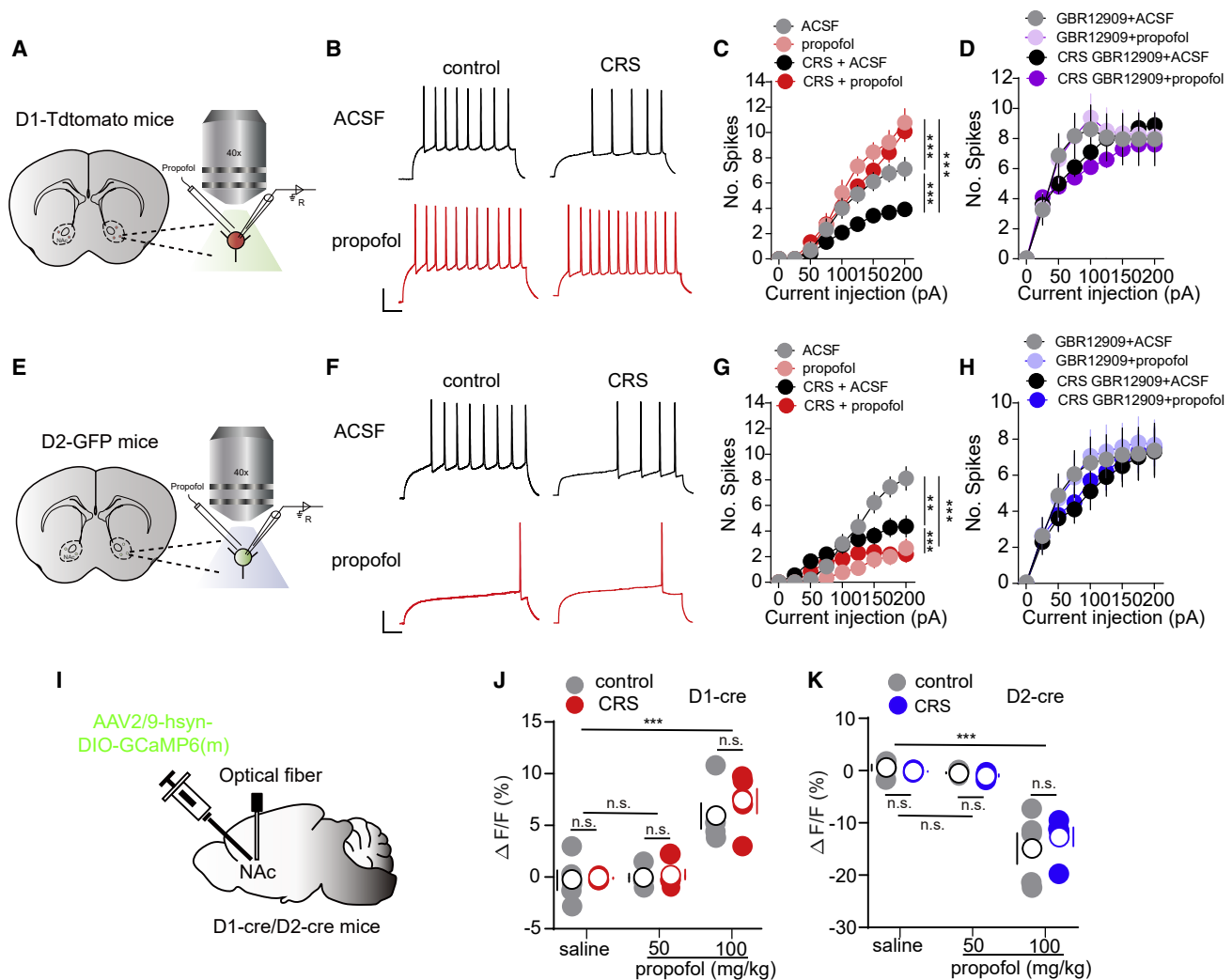
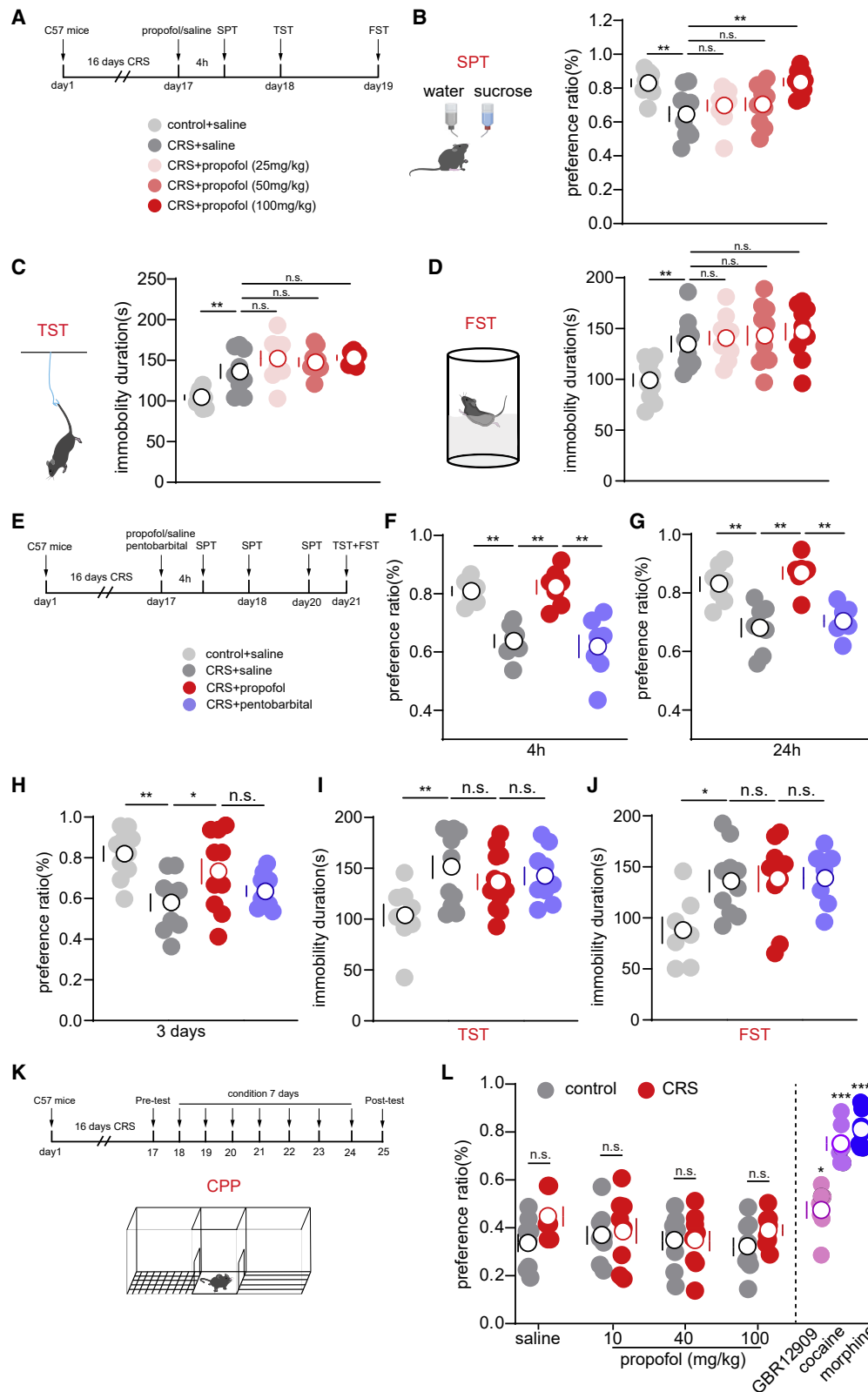


Figure 3. Propofol regulates the activity of NAc MSNs in control and CRS mice

(A) Schematic of whole-cell patch-clamp recording configuration of D1-MSNs in NAc brain slice of D1-tdtomato mice.
 (B) Representative traces of the action potentials recorded from D1-tdtomato neurons in + 200-pA-current injection of control and CRS mice. Scale bars, 20 mV, 50 ms.
 (C) Statistics showed that as the injection current increased (from 0 to + 200 pA), and the number of spikes was significantly increased with perfusion propofol compared with ACSF in D1-tdtomato neurons of control and CRS mice (control group, ACSF, $n = 9$ neurons in 3 mice, propofol, $n = 9$ neurons in 3 mice; CRS group, ACSF, $n = 12$ neurons in 4 mice, propofol, $n = 12$ neurons in 4 mice).
 (D) Statistical analysis showed that the number of spikes was not different between ACSF and propofol perfusion in the presence of GBR12909 (10 μ M) in D1-MSNs of control and CRS mice (control group, ACSF, $n = 13$ neurons in 4 mice, propofol, $n = 13$ neurons in 4 mice; CRS group, ACSF, $n = 10$ neurons in 4 mice, propofol, $n = 10$ neurons in 4 mice).
 (E) Schematic of whole-cell patch-clamp recording configuration of D2-MSNs in NAc brain slice of D2-GFP mice.
 (F) Representative traces of the action potentials recorded from D2-GFP neurons in + 200-pA-current injection of control and CRS mice. Scale bars, 20 mV, 50 ms.
 (G) Statistics showed that as the injection current increased (from 0 to + 200 pA), the number of spikes was significantly decreased with perfusion propofol compared with ACSF in D2-GFP neurons of control and CRS mice (control group, ACSF, $n = 9$ neurons in 3 mice, propofol, $n = 9$ neurons in 3 mice; CRS group, ACSF, $n = 11$ neurons in 4 mice, propofol, $n = 11$ neurons in 4 mice).
 (H) Statistical analysis showed that the number of spikes was not different between ACSF and propofol perfusion in the presence of GBR12909 (10 μ M) in D2-MSNs of control and CRS mice (control group, ACSF, $n = 16$ neurons in 4 mice, propofol, $n = 16$ neurons in 4 mice; CRS group, ACSF, $n = 10$ neurons in 3 mice, propofol, $n = 10$ neurons in 3 mice).
 (I) Schematic of virus injection to express GCaMP6m in the NAc with the optical fiber implanted above the NAc.
 (J and K) Quantification of change in Ca^{2+} signals after administration of saline and propofol (50 and 100 mg/kg) in D1-cre (J) or D2-cre (K) control and CRS mice ($n = 5$ mice for each group). Statistical significance was determined by two-way ANOVA followed by Tukey's multiple comparisons test (C, D, G, H, J, and K). Data are presented as the mean \pm SEM. ** $p < 0.01$; *** $p < 0.001$.
 See also [Figures S4](#), [S5](#), and [S10](#).



(legend on next page)

(Picrotoxin, GABA_A receptor inhibitor) to NAc (Figure S10E) and found that inhibiting D1 receptor but not GABA_A receptor could abolish the anti-anhedonic effect of propofol (Figures 5A–5F), suggesting that GABA_A signaling is not involved in the above observed changes.

To further establish the causal importance of D1-MSNs activation in anhedonia alleviation, we bilaterally infused Cre-dependent AAV-DIO-hM4Di-mCherry and AAV-DIO-mCherry into NAc of D1-Cre mice (Figures 5G and S10F). The perfusion of clozapine N-oxide (CNO) on brain slices selectively reduced the firing rate of D1-MSNs (Figure 5H). The administration of CNO (5 mg/kg) to mice 30 min before propofol blocked the therapeutic effects of propofol (Figures 5I and 5J), suggesting that the activation of D1-MSNs is critical for propofol's effect on anhedonia.

DISCUSSION

This study reported the effect of propofol on accumbal dopamine through its direct binding to DAT. Propofol was found to elevate dopamine levels and activate D1-MSNs, which is required for anhedonia improvement. The results provide insights into the independent behavioral phenotypes underlying depression and raise the possibility of discovering new treatments for anhedonia by screening novel DAT inhibitors with controllable risk for addiction.

The binding mode of DAT-cocaine indicated a binding pocket deeply buried in the transporter structure, overlapping with that of dopamine.²⁰ In this work, we found that propofol is a novel DAT inhibitor. The propofol's low molecule weight and lack of the common positively charged group, compared with the other reported competitive DAT inhibitors such as cocaine and GBR12909, implies that it may have a different molecular mechanism from other DAT inhibitors. Indeed, we found that propofol occupied the transport channel of DAT to block the entry of substrates. Notably, our study identified three critical binding sites (A81, F155, D475) of propofol in DAT that could block propofol binding without affecting dopamine transport. It is worth mentioning that the ligand efficiency²¹ of propo-

fol (0.58) is higher than that of the reported highly active inhibitor BTCP (0.54), suggesting the potentially favorable pocket druggability of this binding site. Last but not least, propofol exhibited little to no affinity for SERT, which is different from cocaine.²²

This evidence establishes the possibility of producing a safer, non-addictive, and non-anesthetic agent against anhedonia through careful chemical design.

In our current practice, the efficiency of propofol is pronounced at sedative dosage; the reduction of the anesthetic effect through structure-based discovery²³ may enhance its at-home application for outpatients. The next step will be engineering a propofol analog based on principles of function-oriented synthesis,²⁴ which could broadly expand and translate our present findings to clinical practices.

It should also be noted that propofol has been reported with abuse potential. Several studies have reported the rapid growth rate of propofol abuse among healthcare workers during the past 10 years, associated with a high mortality rate (~30%),^{25–27} primarily due to rapid injection-induced respiratory depression.^{28,29} Some case reports indicated that propofol might become highly addictive to specific individuals.³⁰ In animal studies, a chronic dosing paradigm (19 days) could induce conditional preference in rats,³¹ while intravenous injection of propofol over 14 days established self-administration behavior.^{32,33} It has been proposed that both the dopamine system and the activation of GABA_A receptors are involved in the formation of addictive behaviors to propofol.^{34,35} In this study, we examined the addiction vulnerability to propofol in both control and chronic stress mice, and found that the seven-dosing paradigms did not induce CPP formation in these animals. We consequently propose that, at the current dosage and single-dose paradigm, the addictive potential of propofol is limited and may not dampen its clinical usage. However, future studies are warranted to validate the safety guidelines for using propofol as a clinical treatment for anhedonia.

In conclusion, the study reveals that propofol may treat anhedonia, one major symptom of depression, by inhibiting DAT.

Figure 4. Propofol reverses anhedonia in CRS mice

(A) Experimental procedure and different drug administration schemes.

(B) Sucrose preference ratio of CRS mice (STAR Methods) among control, saline, and propofol (25, 50, and 100 mg/kg) groups at 4 h after intraperitoneal injection with a single dose (n = 10 mice for each group).

(C and D) Quantifications of performance on TST and FST showing that the immobility durations were not significantly different between saline and propofol groups. Same sample size as in (B).

(E) Experimental procedure and different drug administration schemes.

(F–H) Sucrose preference ratio of mice among control, saline, propofol and pentobarbital groups at 4 h (F) (n = 7 mice for each group), 24 h (G) (n = 7 mice for each group), and 3 days (H) (n = 10 mice for each group) after intraperitoneal injection with a single dose.

(I and J) Quantifications of performance on TST (I) and FST (J) (same sample size as in H) showed that the immobility durations were not significantly different between groups.

(K) Experimental procedure and different drug administration schemes for CPP test.

(L) Mice that received alternating injections of GBR12909, cocaine, morphine, and saline for 7 days showed a significant preference for the GBR12909 (10 mg/kg), cocaine (15 mg/kg), and morphine (15 mg/kg) paired chamber, but mice that received alternating injections of propofol for 7 days showed no preference for the propofol-paired chamber (saline group, control n = 8 mice, CRS n = 6 mice; propofol (10 mg/kg) group, control n = 8 mice, CRS n = 8 mice; propofol (40 mg/kg) group, control n = 8 mice, CRS n = 8 mice; propofol (100 mg/kg) group, control n = 8 mice, CRS n = 8 mice; GBR12909 (10 mg/kg), n = 7 mice; cocaine (15 mg/kg), n = 7 mice; morphine (15 mg/kg), n = 7 mice). Statistical significance was determined by two-way ANOVA followed by Dunnett's multiple comparisons test (B–D, F–J, and L-left panel) and one-way ANOVA followed by Tukey's multiple comparisons test (L-right panel). Data are presented as the mean ± SEM. *p < 0.05; **p < 0.01; ***p < 0.001.

See also Figures S6–S10.

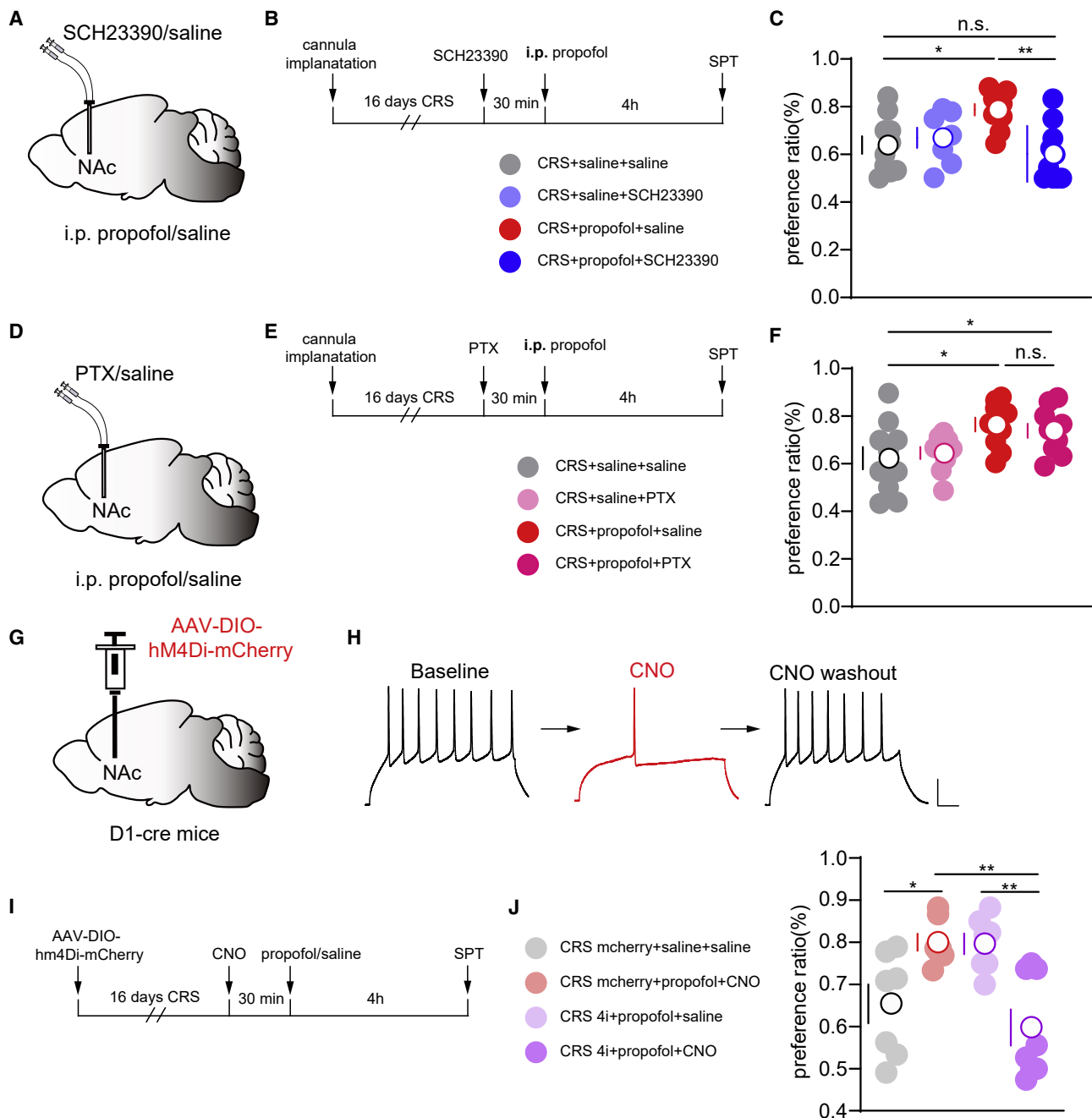


Figure 5. Propofol rapidly attenuates anhedonia through NAc D1-MSNs activation

(A) Schematic of bilateral implantation of cannulae for saline and SCH23390 (2.5 mg/mL) in the NAc.
(B) Experimental procedure and different drug administration schemes.
(C) Sucrose preference ratio of mice among saline + saline, saline + SCH23390, propofol + saline, and propofol + SCH23390 groups (saline + saline, n = 10 mice, saline + SCH23390, n = 7 mice, propofol + saline, n = 10 mice, propofol + SCH23390, n = 10 mice).
(D) Schematic of bilateral implantation of cannulae for saline and PTX (0.5 mg/mL) in NAc.
(E) Experimental procedure and different drug administration schemes.
(F) Sucrose preference ratio of mice among saline + saline, saline + PTX, propofol + saline and propofol + PTX groups (saline + saline, n = 10 mice, saline + PTX, n = 9 mice, propofol + saline, n = 10 mice, propofol + PTX, n = 10 mice).
(G) Schematic of virus injection to express hM4Di in NAc.
(H) Representative traces of the action potentials recorded from mCherry-labeled neurons in + 200-pA-current injection before and after CNO perfusion (5 μ M). Scale bars, 20 mV, 50 ms.

(legend continued on next page)

STAR★METHODS

Detailed methods are provided in the online version of this paper and include the following:

- **KEY RESOURCES TABLE**
- **RESOURCE AVAILABILITY**
 - Lead contact
 - Materials availability
 - Data and code availability
- **EXPERIMENTAL MODEL AND SUBJECT DETAILS**
 - Animals
- **METHOD DETAILS**
 - Drug administration
 - Filtration-based radioligand binding assay
 - [³H] DA Uptake assay
 - Molecular docking of mDAT and ligand complexes
 - Molecular dynamics simulation
 - Live cell imaging of ASP+
 - Fluorescence imaging of DA1m (GRAB_{DA1m}) in cultured cells
 - 18F-FP-CIT PET
 - Stereotactic surgery
 - Fiber photometry
 - Brain slice electrophysiology
 - Western immunoblots
 - Behavioral assays
- **QUANTIFICATION AND STATISTICAL ANALYSIS**

SUPPLEMENTAL INFORMATION

Supplemental information can be found online at <https://doi.org/10.1016/j.neuron.2023.02.017>.

ACKNOWLEDGMENTS

This work was supported by STI2030-Major Projects (2021ZD0203900) to X.-N.Z., The National Natural Science Foundation of China grant (32192414, 61890951, and 31922029), and the Hefei National Research Center for Physical Sciences at the Microscale (KF2021006) to J.H. We would like to thank all members of Hu lab at ShanghaiTech University and Yuan lab at the Shanghai Mental Health Center, Shanghai Jiaotong University School of Medicine. We especially thank J.-J.C., F.B., S.-W.Z., and Y.-R.W. for molecular docking and molecular pharmacology experiments. We also appreciate all the members of the Molecular Imaging Core Facility and Molecular and Cellular Biology Core Facility at ShanghaiTech University for their generous help with this project.

AUTHOR CONTRIBUTIONS

J.H., T.-F.Y., T.X., and X.-N.Z. conceptualized this study and conducted the experimental design, investigation, and analyses. X.-N.Z. performed the radioligand binding, PET scanning, and the brain slice electrophysiology experiments. J.L. and K.-X.Y. performed behavioral tasks and *in vivo* fiber photometry recording experiments. Y.-G.G., J.L., F.C., C.L., and G.-L.Q. performed *in vivo* fiber photometry recording and the immunohistochemical experiments. L.W. performed molecular docking and molecular dynamic experiments. The initial manuscript was prepared by J.H., T.-F.Y., T.X., and X.-N.Z. with further editing

by J.H., T.-F.Y., T.X., and X.-N.Z. Data presentation and visualization was conducted by X.-N.Z., J.L., and G.-L.Q. Project administration was carried out by J.H., T.-F.Y., X.-N.Z., and T.X. Supervision of research was carried out by J.H., T.-F.Y., and T.X., and funding acquisition was carried out by J.H. and X.-N.Z.

DECLARATION OF INTERESTS

The authors declare no competing interests.

INCLUSION AND DIVERSITY

We support inclusive, diverse, and equitable conduct of research.

Received: May 9, 2022

Revised: December 2, 2022

Accepted: February 10, 2023

Published: March 13, 2023

REFERENCES

1. Xiong, J., Lipsitz, O., Nasri, F., Lui, L.M.W., Gill, H., Phan, L., Chen-Li, D., Jacobucci, M., Ho, R., Majeed, A., and McIntyre, R.S. (2020). Impact of COVID-19 pandemic on mental health in the general population: A systematic review. *J. Affect. Disord.* 277, 55–64. <https://doi.org/10.1016/j.jad.2020.08.001>.
2. Snaith, R.P. (1993). Identifying depression: the significance of anhedonia. *Hosp. Pract. (Off Ed)* 28, 55–60. <https://doi.org/10.1080/21548331.1993.11442922>.
3. Craske, M.G., Meuret, A.E., Ritz, T., Treanor, M., and Dour, H.J. (2016). Treatment for anhedonia: A neuroscience driven approach. *Depress. Anxiety* 33, 927–938. <https://doi.org/10.1002/da.22490>.
4. Pizzagalli, D.A., Holmes, A.J., Dillon, D.G., Goetz, E.L., Birk, J.L., Bogdan, R., Dougherty, D.D., Iosifescu, D.V., Rauch, S.L., and Fava, M. (2009). Reduced caudate and nucleus accumbens response to rewards in unmedicated individuals with major depressive disorder. *Am. J. Psychiatry* 166, 702–710. <https://doi.org/10.1176/appi.ajp.2008.08081201>.
5. Lim, B.K., Huang, K.W., Grueter, B.A., Rothwell, P.E., and Malenka, R.C. (2012). Anhedonia requires MC4R-mediated synaptic adaptations in nucleus accumbens. *Nature* 487, 183–189. <https://doi.org/10.1038/nature11160>.
6. Gerfen, C.R., Engber, T.M., Mahan, L.C., Susel, Z., Chase, T.N., Monsma, F.J., Jr., and Sibley, D.R. (1990). D1 and D2 dopamine receptor-regulated gene expression of striatonigral and striatopallidal neurons. *Science* 250, 1429–1432. <https://doi.org/10.1126/science.2147780>.
7. Chandra, R., Francis, T.C., Konkalmatt, P., Amgalan, A., Gancarz, A.M., Dietz, D.M., and Lobo, M.K. (2015). Opposing role for Egr3 in nucleus accumbens cell subtypes in cocaine action. *J. Neurosci.* 35, 7927–7937. <https://doi.org/10.1523/JNEUROSCI.0548-15.2015>.
8. Brechmann, T., Maier, C., Kaisler, M., Vollert, J., Schmiegel, W., Pak, S., Scherbaum, N., Rist, F., and Riphaus, A. (2018). Propofol sedation during gastrointestinal endoscopy arouses euphoria in a large subset of patients. *United European Gastroenterol. J.* 6, 536–546. <https://doi.org/10.1177/2050640617736231>.
9. Pain, L., Gobaille, S., Schleef, C., Aunis, D., and Oberling, P. (2002). *In vivo* dopamine measurements in the nucleus accumbens after nonanesthetic and anesthetic doses of propofol in rats. *Anesth. Analg.* 95, 915–919. <https://doi.org/10.1097/0000539-200210000-00022>.
10. Faraone, S.V., Spencer, T.J., Madras, B.K., Zhang-James, Y., and Biederman, J. (2014). Functional effects of dopamine transporter gene

(I) Experimental procedure and different drug administration schemes.

(J) Sucrose preference ratio of mice among saline, propofol, propofol + mcherry, and propofol + hM4Di groups (n = 7 mice per group). Statistical significance was determined by two-way ANOVA followed by Tukey's multiple comparisons test. Data are presented as the mean ± SEM. *p < 0.05; **p < 0.01.

See also [Figure S10](#).

- genotypes on in vivo dopamine transporter functioning: a meta-analysis. *Mol. Psychiatry* 19, 880–889. <https://doi.org/10.1038/mp.2013.126>.
11. Bonvicini, C., Faraone, S.V., and Scassellati, C. (2016). Attention-deficit hyperactivity disorder in adults: a systematic review and meta-analysis of genetic, pharmacogenetic and biochemical studies. *Mol. Psychiatry* 21, 1643. <https://doi.org/10.1038/mp.2016.128>.
12. Sambo, D.O., Lin, M., Owens, A., Lebowitz, J.J., Richardson, B., Jagnarine, D.A., Shetty, M., Rodriguez, M., Alonge, T., Ali, M., et al. (2017). The sigma-1 receptor modulates methamphetamine dysregulation of dopamine neurotransmission. *Nat. Commun.* 8, 2228. <https://doi.org/10.1038/s41467-017-02087-x>.
13. Chen, N., Zhen, J., and Reith, M.E. (2004). Mutation of Trp84 and Asp313 of the dopamine transporter reveals similar mode of binding interaction for GBR12909 and benztropine as opposed to cocaine. *J. Neurochem.* 89, 853–864. <https://doi.org/10.1111/j.1471-4159.2004.02386.x>.
14. Krasowski, M.D., Jenkins, A., Flood, P., Kung, A.Y., Hopfinger, A.J., and Harrison, N.L. (2001). General anesthetic potencies of a series of propofol analogs correlate with potency for potentiation of gamma-aminobutyric acid (GABA) current at the GABA(A) receptor but not with lipid solubility. *J. Pharmacol. Exp. Ther.* 297, 338–351.
15. Sun, F., Zeng, J., Jing, M., Zhou, J., Feng, J., Owen, S.F., Luo, Y., Li, F., Wang, H., Yamaguchi, T.J.C., et al. (2018). A genetically encoded fluorescent sensor enables rapid and specific detection of dopamine in flies, fish, and mice. *Cell* 174, 481.e19–496.e19.
16. Wan, J., Peng, W., Li, X., Qian, T., Song, K., Zeng, J., Deng, F., Hao, S., Feng, J., Zhang, P., et al. (2021). A genetically encoded sensor for measuring serotonin dynamics. *Nat. Neurosci.* 24, 746–752. <https://doi.org/10.1038/s41593-021-00823-7>.
17. Li, K.Y., Xiao, C., Xiong, M., Delphin, E., and Ye, J.H. (2008). Nanomolar propofol stimulates glutamate transmission to dopamine neurons: a possible mechanism of abuse potential? *J. Pharmacol. Exp. Ther.* 325, 165–174. <https://doi.org/10.1124/jpet.107.132472>.
18. Soares-Cunha, C., de Vasconcelos, N.A.P., Coimbra, B., Domingues, A.V., Silva, J.M., Loureiro-Campos, E., Gaspar, R., Sotiropoulos, I., Sousa, N., and Rodrigues, A.J. (2020). Nucleus accumbens medium spiny neurons subtypes signal both reward and aversion. *Mol. Psychiatry* 25, 3241–3255. <https://doi.org/10.1038/s41380-019-0484-3>.
19. Zacny, J.P., Lichter, J.L., Thompson, W., and Apfelbaum, J.L. (1993). Propofol at a subanesthetic dose may have abuse potential in healthy volunteers. *Anesth. Analg.* 77, 544–552. <https://doi.org/10.1213/00005539-199309000-00020>.
20. Beuming, T., Kniazeff, J., Bergmann, M.L., Shi, L., Gracia, L., Raniszewska, K., Newman, A.H., Javitch, J.A., Weinstein, H., Gether, U., and Loland, C.J. (2008). The binding sites for cocaine and dopamine in the dopamine transporter overlap. *Nat. Neurosci.* 11, 780–789. <https://doi.org/10.1038/nn.2146>.
21. Kuntz, I.D., Chen, H., Sharp, K.A., and Kollman, P.A. (1999). The maximal affinity of ligands. *Proc. Natl. Acad. Sci. USA* 96, 9997–10002. <https://doi.org/10.1073/pnas.96.18.9997>.
22. Li, Y., Simmler, L.D., Van Zessen, R., Flakowski, J., Wan, J.X., Deng, F., Li, Y.L., Nautiyal, K.M., Pascoli, V., and Lüscher, C. (2021). Synaptic mechanism underlying serotonin modulation of transition to cocaine addiction. *Science* 373, 1252–1256. <https://doi.org/10.1126/science.abi9086>.
23. Cao, D., Yu, J., Wang, H., Luo, Z., Liu, X., He, L., Qi, J., Fan, L., Tang, L., Chen, Z., et al. (2022). Structure-based discovery of nonhallucinogenic psychedelic analogs. *Science* 375, 403–411. <https://doi.org/10.1126/science.abl8615>.
24. Cameron, L.P., Tombari, R.J., Lu, J., Pell, A.J., Hurley, Z.Q., Ehinger, Y., Vargas, M.V., McCarroll, M.N., Taylor, J.C., Myers-Turnbull, D., et al. (2021). A non-hallucinogenic psychedelic analogue with therapeutic potential. *Nature* 589, 474–479. <https://doi.org/10.1038/s41586-020-3008-z>.
25. Cho, H.Y., Hwang, Y., Shin, S., Yoon, S., and Lee, H.J. (2022). Propofol abuse among healthcare workers: an analysis of criminal cases using the database of the Supreme Court of South Korea's judgments. *Korean J. Anesthesiol.* 75, 391–396. <https://doi.org/10.4097/kja.21507>.
26. Gwiazda, S., Dixon, E., Cronly, M., Kavanagh, Y., Cullinane, M., and Mulligan, L.M. (2021). Propofol misuse in Ireland - two case reports and a review of the literature. *Forensic Sci. Int.* 326, 110909. <https://doi.org/10.1016/j.forsciint.2021.110909>.
27. Han, E., Jung, S., Baek, S., Lee, S., and Chung, H. (2013). Deaths from recreational use of propofol in Korea. *Forensic Sci. Int.* 233, 333–337. <https://doi.org/10.1016/j.forsciint.2013.10.008>.
28. Klausz, G., Róna, K., Kristóf, I., and Tőro, K. (2009). Evaluation of a fatal propofol intoxication due to self administration. *J. Forensic Leg. Med.* 16, 287–289. <https://doi.org/10.1016/j.jflm.2008.12.010>.
29. Iwersen-Bergmann, S., Rösner, P., Kühnau, H.C., Junge, M., and Schmoldt, A. (2001). Death after excessive propofol abuse. *Int. J. Legal Med.* 114, 248–251. <https://doi.org/10.1007/s004149900129>.
30. Bonnet, U., and Scherbaum, N. (2012). Craving dominates propofol addiction of an affected physician. *J. Psychoactive Drugs* 44, 186–190. <https://doi.org/10.1080/02791072.2012.684635>.
31. Shahzadi, A., Uskur, T., Akkan, A.G., Çevreli, B., and Uzbay, T. (2018). Effects of propofol on conditioned place preference in male rats: involvement of nitergic system. *Am. J. Drug Alcohol Abuse* 44, 167–174. <https://doi.org/10.1080/00952990.2017.1344681>.
32. LeSage, M.G., Stafford, D., and Glowa, J.R. (2000). Abuse liability of the anesthetic propofol: self-administration of propofol in rats under fixed-ratio schedules of drug delivery. *Psychopharmacol. (Berl.)* 153, 148–154. <https://doi.org/10.1007/s002130000430>.
33. Weerts, E.M., Ator, N.A., and Griffiths, R.R. (1999). Comparison of the intravenous reinforcing effects of propofol and methohexital in baboons. *Drug Alcohol Depend.* 57, 51–60. [https://doi.org/10.1016/s0376-8716\(99\)00044-7](https://doi.org/10.1016/s0376-8716(99)00044-7).
34. Yang, B., Wang, B.F., Lai, M.J., Zhang, F.Q., Yang, X.W., Zhou, W.H., and Lian, Q.Q. (2011). Differential involvement of GABAA and GABAB receptors in propofol self-administration in rats. *Acta Pharmacol. Sin.* 32, 1460–1465. <https://doi.org/10.1038/aps.2011.123>.
35. Wang, S., Wang, X., Lin, W., Bao, S., Wang, B., Wu, B., Su, Y., and Lian, Q. (2018). Dopamine D(1) receptor within basolateral amygdala is involved in propofol relapse behavior induced by cues. *Neurochem. Res.* 43, 2393–2403. <https://doi.org/10.1007/s11064-018-2667-8>.
36. Fan, Z., Chang, J., Liang, Y., Zhu, H., Zhang, C., Zheng, D., Wang, J., Xu, Y., Li, Q.J., and Hu, H. (2023). Neural mechanism underlying depressive-like state associated with social status loss. *Cell* 186, 560.e17–576.e17. <https://doi.org/10.1016/j.cell.2022.12.033>.
37. Li, K., Zhou, T., Liao, L., Yang, Z., Wong, C., Henn, F., Malinow, R., Yates, J.R., 3rd, and Hu, H. (2013). betaCaMKII in lateral habenula mediates core symptoms of depression. *Science* 341, 1016–1020. <https://doi.org/10.1126/science.1240729>.
38. Yang, Y., Cui, Y., Sang, K., Dong, Y., Ni, Z., Ma, S., and Hu, H. (2018). Ketamine blocks bursting in the lateral habenula to rapidly relieve depression. *Nature* 554, 317–322. <https://doi.org/10.1038/nature25509>.
39. Xi, Z.X., Song, R., Li, X., Lu, G.Y., Peng, X.Q., He, Y., Bi, G.H., Sheng, S.P., Yang, H.J., Zhang, H., et al. (2017). CTDp-32476: a promising agonist therapy for treatment of cocaine addiction. *Neuropsychopharmacology* 42, 682–694. <https://doi.org/10.1038/npp.2016.155>.
40. Jin, Z.L., Gao, N., Zhou, D., Chi, M.G., Yang, X.M., and Xu, J.P. (2012). The extracts of *Fructus Akebiae*, a preparation containing 90% of the active ingredient hederagenin: serotonin, norepinephrine and dopamine reuptake inhibitor. *Pharmacol. Biochem. Behav.* 100, 431–439. <https://doi.org/10.1016/j.pbb.2011.10.001>.
41. Ishibashi, T., Horisawa, T., Tokuda, K., Ishiyama, T., Ogasa, M., Tagashira, R., Matsumoto, K., Nishikawa, H., Ueda, Y., Toma, S., et al. (2010). Pharmacological profile of lurasidone, a novel antipsychotic agent with potent 5-hydroxytryptamine 7 (5-HT7) and 5-HT1A receptor activity.

- J. Pharmacol. Exp. Ther. 334, 171–181. <https://doi.org/10.1124/jpet.110.167346>.
42. Mason, J.N., Farmer, H., Tomlinson, I.D., Schwartz, J.W., Savchenko, V., DeFelice, L.J., Rosenthal, S.J., and Blakely, R.D. (2005). Novel fluorescence-based approaches for the study of biogenic amine transporter localization, activity, and regulation. *J. Neurosci. Methods* 143, 3–25. <https://doi.org/10.1016/j.jneumeth.2004.09.028>.
43. Swant, J., Goodwin, J.S., North, A., Ali, A.A., Gamble-George, J., Chirwa, S., and Khoshbouei, H. (2011). Alpha-synuclein stimulates a dopamine transporter-dependent chloride current and modulates the activity of the transporter. *J. Biol. Chem.* 286, 43933–43943. <https://doi.org/10.1074/jbc.M111.241232>.
44. Yuan, Y., Wu, W., Chen, M., Cai, F., Fan, C., Shen, W., Sun, W., and Hu, J. (2019). Reward inhibits paraventricular CRH neurons to relieve stress. *Curr. Biol.* 29, 1243.e4–1251.e4. <https://doi.org/10.1016/j.cub.2019.02.048>.
45. Loureiro, M., Achargui, R., Flakowski, J., Van Zessen, R., Stefanelli, T., Pascoli, V., and Lüscher, C. (2019). Social transmission of food safety depends on synaptic plasticity in the prefrontal cortex. *Science* 364, 991–995. <https://doi.org/10.1126/science.aaw5842>.
46. Mohebi, A., Pettibone, J.R., Hamid, A.A., Wong, J.T., Vinson, L.T., Patriarchi, T., Tian, L., Kennedy, R.T., and Berke, J.D. (2019). Dissociable dopamine dynamics for learning and motivation. *Nature* 570, 65–70. <https://doi.org/10.1038/s41586-019-1235-y>.
47. Li, J., Lu, C., Gao, Z., Feng, Y., Luo, H., Lu, T., Sun, X., Hu, J., and Luo, Y. (2020). SNRIs achieve faster antidepressant effects than SSRIs by elevating the concentrations of dopamine in the forebrain. *Neuropharmacology* 177, 108237. <https://doi.org/10.1016/j.neuropharm.2020.108237>.
48. Tye, K.M., Mirzabekov, J.J., Warden, M.R., Ferenczi, E.A., Tsai, H.C., Finkelstein, J., Kim, S.Y., Adhikari, A., Thompson, K.R., Andelman, A.S., et al. (2013). Dopamine neurons modulate neural encoding and expression of depression-related behaviour. *Nature* 493, 537–541. <https://doi.org/10.1038/nature11740>.
49. Powell, T.R., Fernandes, C., and Schalkwyk, L.C. (2012). Depression-related behavioral tests. *Curr. Protoc. Mouse Biol.* 2, 119–127. <https://doi.org/10.1002/9780470942390.mo110176>.
50. Can, A., Dao, D.T., Terrillion, C.E., Piantadosi, S.C., Bhat, S., and Gould, T.D. (2012). The tail suspension test. *J. Vis. Exp.* e3769.
51. Li, Y., Li, C.Y., Xi, W., Jin, S., Wu, Z.H., Jiang, P., Dong, P., He, X.B., Xu, F.Q., Duan, S., et al. (2019). Rostral and caudal ventral tegmental area GABAergic inputs to different dorsal raphe neurons participate in opioid dependence. *Neuron* 101, 748.e5–761.e5. <https://doi.org/10.1016/j.neuron.2018.12.012>.
52. Su, X.Y., Chen, M., Yuan, Y., Li, Y., Guo, S.S., Luo, H.Q., Huang, C., Sun, W., Li, Y., Zhu, M.X., et al. (2019). Central processing of itch in the midbrain reward center. *Neuron* 102, 858.e5–872.e5. <https://doi.org/10.1016/j.neuron.2019.03.030>.
53. Jiang-Xie, L.F., Yin, L., Zhao, S., Prevosto, V., Han, B.X., Dzirasa, K., and Wang, F. (2019). A common neuroendocrine substrate for diverse general anesthetics and sleep. *Neuron* 102, 1053.e4–1065.e4. <https://doi.org/10.1016/j.neuron.2019.03.033>.
54. Simmler, L.D., Li, Y., Hadjas, L.C., Hiver, A., van Zessen, R., and Lüscher, C. (2022). Dual action of ketamine confines addiction liability. *Nature* 608, 368–373. <https://doi.org/10.1038/s41586-022-04993-7>.

STAR★METHODS

KEY RESOURCES TABLE

REAGENT or RESOURCE	SOURCE	IDENTIFIER
Antibodies		
Anti-Dopamine Transporter Antibody	Alomone labs	Cat#AMT-003; RRID:AB_10687463
Chemicals, peptides, and recombinant proteins		
Propofol	ApexBio	Cat#C6265
BTCP	Sigma	Cat#B138
Imipramine	Sigma	Cat#I0899
2,6-Dimethylthiophenol	Aladdin	Cat#D103093
2,6-Dimethoxyphenol	Aladdin	Cat#D128348
2,6-Dibromophenol	Aladdin	Cat#D130206
1,3-Diisopropylbenzene	Aladdin	Cat#D155022
2,4-Di-tert-butylphenol	Aladdin	Cat#D104351
2-Cyclopentylphenol	Santa Cruz	Cat#sc225332
2-Hydroxy-3-isopropylbenzoic acid	Santa Cruz	Cat#sc230379
Clozapine N-oxide(CNO)	ENZO	Cat#BML-NS105-0025
GBR12909	MedChemExpress	Cat#HY-13217A
Cocaine	Qinghai Pharmaceutical Firm	N/A
Morphine	Northeast pharmaceutical group Shenyang	N/A
SCH23390	ApexBio	Cat#M9099
PTX	Tocris Bioscience	Cat#1128
Sulpiride	MedChemExpress	Cat#HY-B1019
4-Di-1-ASP(4-(4-(dimethylamino)styryl) Nmethylpyridinium Iodide) (ASP+)	Invitrogen	Cat#D288
Deposited data		
DAT template	PDB	ID : 4XP1
Experimental models: Cell lines		
HEK-293	National Collection of Authenticated Cell Cultures	GNHu 43
Experimental models: Organisms/strains		
DAT-ires-cre	Jackson Laboratory (USA)	JAX: 006660
D1-Cre	MMRRC	017264-UCD
D2-Cre	MMRRC	017263-UCD
D1-tdTomato	Jackson Laboratory (USA)	JAX:016204
D2-GFP	Jackson Laboratory (USA)	JAX:030537
C57BL/6J	Silaike Experiment Animal Co., Ltd. (Shanghai)	JAX: 000664
Oligonucleotides		
shRNA targeting sequence: DAT: GCCCATTTATGCCACCTATAA	This paper	N/A
Recombinant DNA		
AAV-hSyn-DA1m-WPRE-PA	Wuhan BrainVTA Co.	N/A
AAV-hSyn-5HT1.0-WPRE-PA	Wuhan BrainVTA Co.	N/A
AAV-EF1 α -DIO-GCaMP6m	Wuhan BrainVTA Co.	N/A
AAV-DIO-hM4Di-mCherry	Wuhan BrainVTA Co.	N/A
AAV-DIO-mCherry	Wuhan BrainVTA Co.	N/A

(Continued on next page)

Continued

REAGENT or RESOURCE	SOURCE	IDENTIFIER
retro-AAV -shRNA- DAT-EGFP	OBiO Technology (Shanghai) Corp, Ltd.	N/A
retro-AAV -shRNA- scramble-EGFP	OBiO Technology (Shanghai) Corp, Ltd.	N/A
pdisplay-GRAB-DA1m-EGFP-CAAX	Sun et al. ¹⁵	N/A
Software and algorithms		
Digbehav video-recording software	Jiliang, Shanghai, China	http://www.ecgonline.cn/main.asp
Spike2 software	CED	N/A
MATLAB	MathWorks	https://www.mathworks.com/
Prime	Schrödinger LLC	https://www.schrodinger.com/products/prime
Glide	Schrödinger LLC	https://www.schrodinger.com/products/glide
Desmond	Schrödinger LLC	https://www.schrodinger.com/products/desmond
NIKON-NIS-ELEMENTS software	Nikon Corporation	N/A
Image J	NIH Image	RRID: SCR_003070
GraphPad Prism 8.0	GraphPad	https://www.graphpad.com/scientific-software/prism/

RESOURCE AVAILABILITY

Lead contact

Further information and requests for reagents may be directed to and will be fulfilled by the corresponding author Ji Hu (huji@shanghaitech.edu.cn).

Materials availability

This study did not generate new unique reagents or mouse lines.

Data and code availability

- All raw data reported in this paper will be shared by the [lead contact](#) upon request.
- The original code reported in this paper is provided in [Table S3](#).
- Any additional information required to reanalyze the data reported in this paper is available from the [lead contact](#) upon request.

EXPERIMENTAL MODEL AND SUBJECT DETAILS

Animals

Male and female C57BL/6J, DAT-ires-cre, D1-tdTomato transgenic, D2-GFP transgenic, D1-Cre and D2-Cre mice aged 6-8 weeks were used for the experiments. Half male and half female mice were used for *in vivo* fiber photometry recordings and *in vitro* electrophysiological recordings. According to previous studies, we only included male mice in the CRS procedure and behavioral tasks to reduce the confounding factors induced by hormonal fluctuations in behavioral experiments.³⁶⁻³⁸ All mice were maintained 4-5 per cage under a 12h light-dark cycle (light on from 7:00 a.m. to 7:00 p.m.) at 22–25 °C with free access to food and water. The mice strains were listed in the [key resources table](#). Experiments were performed exactly as approved by the IACUC at ShanghaiTech University.

METHOD DETAILS

Drug administration

For systemic drug delivery, propofol (ApexBio, C6265) was dissolved in DMSO and further diluted with 0.9% saline. GBR12909 dihydrochloride (MedChemExpress, HY-13217A), cocaine (Qinghai Pharmaceutical Firm), and morphine (Northeast Pharmaceutical Group Shenyang, China) were dissolved in 0.9% saline. All drugs were administered intraperitoneally (i.p.) for behavioral testing or *in vivo* fiber photometry recording, or prior to sacrificing mice for *in vitro* electrophysiology studies. For cannulae infusion and chemogenetic experiments in freely behaving mice, D1 receptor antagonist SCH23390 (ApexBio, M9099), GABA_A receptor antagonist PTX (Tocris Bioscience, 1128), and Clozapine-N-oxide (CNO) (ENZO, BML-NS105-0025) were dissolved in 0.2 mL vehicle solution (PBS with 0.3% DMSO).

Filtration-based radioligand binding assay

The cell membrane preparation process was modified from a previous report.³⁹ The membranes were prepared from human embryonic kidney 293 (HEK293 cells), stably expressing DATs and SERTs. The affinities of the test compounds, BTCP (Sigma-B138) and

imipramine (Sigma-I0899) as positive controls, propofol, and its analogs (2,6-Dimethylthiophenol, Aladdin-D103093; 2,6-Dimethoxyphenol, Aladdin-D128348; 2,6-Dibromophenol, Aladdin-D130206; 1,3-Diisopropylbenzene, Aladdin-D155022; 2,4-Di-tert-butylphenol, Aladdin-D104351; 2-Cyclopentylphenol, Santa Cruz-sc225332; 2-Hydroxy-3-isopropylbenzoic acid, Santa Cruz-sc230379) for DAT or SERT were determined by interaction with [³H] CFT (WIN 35,428 from PE-NET1033250UC),⁴⁰ [³H]GBR12935 (PE-NET918) or [³H]imipramine (Sigma-I0899). Briefly, the filtration binding assay was performed in an assay buffer containing 5 μg membrane protein, various concentrations reference compounds and radio-ligands. Nonspecific binding was determined in the presence of an unlabeled ligand at 10 μM (Low control: LC), and total binding was determined with DMSO (High control: HC). The reaction was terminated by filtration through Whatman GF/C filters presoaked in 0.3% polyethyleneimine for 30 min at room temperature. After drying, the filter-bound radioactivity was determined using Perkin Elmer MicroBeta2 Reader by scintillation spectrometry. For the data analysis, we calculated the Inhibition and IC50 values using the following equation: %Inhibition = (1 - (Assay well - Average_LC) / (Average_HC - Average_LC)) * 100% and analyzed the data with Prism 8.0 following the model “log (inhibitor) vs. Variable response slope” to fit the curve. Ki values were calculated according to the Cheng-Prusoff equation⁴¹ (L: radioligand concentration, Kd: dissociation constant, Km: Michaelis-Menten constant).

[³H] DA Uptake assay

[³H] DA uptake assay was conducted exactly as described above for the radio-ligand binding assay except that [³H] WIN 35,428 was replaced with [³H] DA (PE- NET1160001MC). The concentration of [³H] dopamine was 20 nM in this assay.

Molecular docking of mDAT and ligand complexes

We build the homology model of DAT by the advance homology modeling module of Schrödinger2022-4, the template (PDB ID: 4XP1; resolution 2.89 Å) was downloaded from the PDB, the dopamine structure was optimized by the prime module. The homology model was refined by protein preparation wizard and protein-ligand complex refinement module of Schrödinger2022-4, all the options were set to default. The ligand structures of dopamine, propofol, and analogs were prepared by LigPrep of Schrödinger2022-4 and docked to the refined DAT-ligand complex using the Standard Precision (SP) scoring function of glide module of Schrödinger2022-4, the maximum number of output binding pose was set to 10, and the best binding pose was selected by visual inspection. The MM/GBSA binding free energy was calculated by the prime module with the OPLS4 force fields.

Molecular dynamics simulation

A 1000 ns MD simulation was performed using Desmond of Schrödinger2021-2 to optimize the conformation and investigate the binding mode stability of DAT with different ligands. The simulation systems were prepared by applying the OPLS4 force field to the complex and an orthorhombic box was generated by 10 Å border from the complexes. The complex was centered and the transmembrane domain was settled to be wrapped with POPC membrane. Then SPC water molecules were adopted to fill the box while 0.15 M NaCl and additional Na⁺, Cl⁻ were also being added to neutralize the system randomly (the other parameters were set to default values). The molecular dynamics simulations were performed by Desmond under the ensemble (NPT) to maintain the constant temperature (300 K) and pressure (1. 01325 bar).

Live cell imaging of ASP+

Uptake experiments were executed in GFP-DAT HEK 293 cells as previously described^{12,42,43} GFP-DAT Human Embryonic Kidney 293 (HEK 293) cells have been widely used in the field to study DAT biology. To induce expression of DAT and different mutant DAT proteins, cells were transfected using a standard lipofectamine 2000 protocol, and transfected cells were used in experiments 12–36 h after transfection. Then, cells were imaged via a Nikon A1 laser-scanning confocal microscope (Nikon Corporation) at 37 °C in a standard external solution containing: 130 mM NaCl, 10 mM HEPES, 34 mM dextrose, 1.5 mM CaCl₂, 0.5 mM MgSO₄, and 1.3 mM KH₂PO₄ at pH 7.35 and osmolarity of 270 mOsm. Images of GFP-DAT and different DAT mutants were taken at the beginning of each experiment. 4-Di-1-ASP (4-(4-(dimethylamino)styryl) Nmethylpyridinium Iodide) (ASP+) (Invitrogen, D288) was dissolved in external solution. To measure ASP+ uptake, fluorescence was measured at an excitation of 488 nm and emissions of 590/50 nm. Baseline images were acquired for 30s, followed by the addition of ASP+ solution to give a final concentration of 4 μM. Images were acquired for 20 min. For drug treatments, cells were treated with multiple concentrations of propofol for 20 min at 37 °C. For analysis, regions of interest (ROIs) were detected on GFP-DAT images with Image J software (NIH) to encompass the entire internal region of the cell. Background fluorescence was subtracted from each frame. The uptake of ASP+ was determined from the average fluorescent units normalized to the average fluorescence of the first 30 s of baseline imaging for each cell.

Fluorescence imaging of DA1m (GRAB_{DA1m}) in cultured cells

The HEK293 cells were plated on 35-mm glass-bottom dishes and grown to ~50% confluence for transfection. Transfection was performed by incubating the cells with a mixture containing 2-μg DNA ($\text{pdisplay-GRAB-DA1m-EGFP-CAAX}^{15}$) and 6-μg PEI for 6 h. Imaging was performed on a Nikon A1R confocal microscope 48 h after transfection. During imaging, the cultured cells were incubated with a solution containing (in mM): 150 NaCl, 4 KCl, 2 MgCl₂, 2 CaCl₂, 10 HEPES, and 10 glucose (pH 7.4). Solutions containing the drug/compound of interest (DA (Sigma-Aldrich, # 62-31-7), Halo (Tocris, # 0931), propofol (10 μM)) were dripped slowly by

using a gravity-driven superfusion system into the cultured cells. The GFP signals (the GRAB_{DA1m} sensors) were recorded using a 525/50-nm emission filter and analyzed by NIKON-NIS-ELEMENTS software.

18F-FP-CIT PET

The mice pre-anaesthetized with pentobarbital were intraperitoneally injected with propofol (50mg/kg or 100mg/kg) or saline. After 15 min, [18F] FP-CIT was injected into the tail vein with a syringe and then placed in the gantry of the PET scanner (Inveon MM microPET/CT). 10 min CT X-ray for attenuation correction was scanned with a power of 80Kv and 500 uA and an exposure time of 1100 ms before PET scan. A static PET scan investigated tracer accumulation in the brain at 10 min, and images were reconstructed by an OSEM3D (Three-Dimensional Ordered Subsets Expectation Maximum) algorithm followed by MAP (Maximization/Maximum a Posteriori) or FastMAP provided by IAW. The 3D regions of interest (ROIs) were drawn over the brain guided by CT images and tracer uptake was measured using the software of Inveon Research Workplace (IRW) 3.0. Individual quantification of the [18F]-FP-CIT uptake in striatum was calculated. Mean standardized uptake values (SUV) were determined by dividing the relevant ROI concentration by the ratio of the injected activity to the body weight.

Stereotactic surgery

AAV-hSyn-DA1m-WPRE-PA, AAV-hSyn-5HT1.0-WPRE-PA, AAV-EF1 α -DIO-GCaMP6m, AAV-DIO-hM4Di-mCherry, AAV-DIO-mCherry, retro-AAV-shRNA-DAT-GFP and retro-AAV-shRNA-scramble-GFP were purchased from BrainVTA (Wuhan China) and Obio Technology (Shanghai). Optical fibers and cannulae were purchased from RWD Life Science Co., LTD (Shenzhen, China). Surgical procedures were similar to those described by Yuan et al.⁴⁴ In brief, anesthesia was induced with 4% isoflurane (w/v) and maintained at 1.5%. Then mice were placed in a stereotactic apparatus to adjust their skulls to be parallel to the reference panel. For fiber photometry recordings, 300 nL AAV was slowly injected into either NAc unilaterally (coordinates from Bregma: +1.2mmAP, \pm 1.35mmML, 4.0mmDV)^{45,46} and the fiber implantation coordinates were 0.2 mm above the viral injection sites. For chemogenetic manipulations, AAV was slowly injected into NAc bilaterally without fiber implantation. For cannulae implantation, no AAV was injected, and cannulae were implanted into the NAc. In all surgery, the injector was kept still for at least another 10 min to allow viral particles to diffuse.

Fiber photometry

After two weeks of recovery, mice underwent fiber photometry recordings. Fluorescence signals were obtained with a fiber photometry system (488 nm excitation laser, Coherent, # OBIS LS-488; 505-544 nm emission filter and a photomultiplier tube, Thorlabs, # MDF-GFP) and a photomultiplier tube (Hamamatsu, # R3896). The analog voltage signals were digitalized at 100 Hz, and a Power 1401 digitizer and Spike2 software (CED, Cambridge, UK, # 1401) were used to record them. An optical fiber (Thorlabs, # RJPSF2) with an integrated rotary joint preventing fiber damage from animal movement was used to guide the light between the fiber photometry system and the implanted optical fiber. The laser power was adjusted to 20–40 μ W to minimize bleaching. The analysis methods of fiber photometry experiments were as follows. Photometry data were exported to MATLAB R2021a mat files. We first corrected the bleaching of the fluorescence (Table S3). Then, we calculate the values of fluorescence change ($\Delta F/F$), defined as $(F-F_0)/F$, where F_0 is the baseline fluorescence signal averaged over a 300 s-long control time window that is defined as the part where the signal reaches stability after the wire is connected. $\Delta F/F$ values were presented with average plots with a shaded area indicating SEM. To attain the value used for statistics, we calculated the average of $\Delta F/F$ values 3000–5000 s after drug injection as the statistical value of drug treatment.

Brain slice electrophysiology

Adult (6–8 weeks old) male *DAT-ires-cre* mice were injected with AAV2/9-EF1a-DIO-mCherry in the VTA. Two weeks later, D1-tdTomato, D2-GFP transgenic mice and *DAT-ires-cre* mice were subjected to CRS for 16 days, and then they were anesthetized with tribromoethanol (100 mgkg⁻¹, i.p.) and perfused transcardially with ice-cold oxygenated (95% O₂/5% CO₂) NMDG ACSF solution, which included 93 mM NMDG, 93 mM HCl, 2.5 mM KCl, 1.25 mM NaH₂PO₄, 10 mM MgSO₄·7H₂O, 30 mM NaHCO₃, 25 mM glucose, 20 mM HEPES, 5 mM sodium ascorbate, 3 mM sodium pyruvate, and 2 mM thiourea. After perfusion, the brain was rapidly dissected out and immediately transferred into ice-cold oxygenated NMDG ACSF solution. Then we sectioned the coronal plane of brain tissue at 300 μ m in the same buffer using a vibratome (VT1200 S, Leica). The brain slices containing the VTA and NAc were incubated in oxygenated NMDG ACSF at 32°C for 10–15 min, then transferred to a normal oxygenated solution of ACSF (126 mM NaCl, 2.5 mM KCl, 1.25 mM NaH₂PO₄, 2 mM MgSO₄·7H₂O, 10 mM Glucose, 26 mM NaHCO₃, 2 mM CaCl₂) at room temperature for 1h. All chemicals used in slice preparation were purchased from Sigma-Aldrich (St. Louis, MO, USA).

Slices were transferred to the recording chamber that was submerged and superfused with ACSF at a rate of 3 mL/min at 28°C. Whole-cell patch-clamp recordings were made from VTA and NAc neurons visualized with an Olympus BX61W1 microscope (equipped with GFP and mCherry filters) using infrared video microscopy and differential interference contrast optics. VTA DA and NAc D1-TdTomato neurons were identified by mCherry fluorescence, and NAc D2-GFP neurons were identified by GFP fluorescence. The recording pipettes (3–4 M Ω) were prepared with a micropipette puller (P2000, Sutter Instrument; USA). For whole-cell recording, the pipettes were filled with ACSF solution containing 133 mM potassium gluconate, 18 mM NaCl, 0.6 mM EGTA, 10 mM HEPES, 2 mM Mg·ATP, and 0.3 mM Na₃GTP (pH:7.2, 280 mOsm). For action potentials evoked by current injections, a current-step protocol

(from -25 to $+200$ pA, with 25 pA increment for NAc recording and from -50 to $+300$ pA, with 50 pA increment for VTA recording and the step currents during recording of action potential is 400ms) was run and repeated. Then the neurons were held at -70 mV under a voltage-clamp mode to record spontaneous excitatory postsynaptic currents (sEPSCs) for 5 min.

For cell-attach recording, the pipettes were filled with ACSF solution. Cells were held at 0 pA under a current-clamp mode to record spontaneous firing. Propofol (10 μ M) was focally applied by using a gravity-driven superfusion system, and a microinjector coupled to a fine-tip metallic micropipette was placed 50–100 μ m above the recorded neuron followed by 5–10 min of recording. GBR12909 (Tocris Bioscience, United Kingdom; 10 μ M), PTX and Sulpiride (MedChemExpress(MCE); 10 μ M) was diluted in fresh ACSF until completely mixed and then transferred to separate graduated reservoirs connected to the chamber (1 to 2 ml/min) respectively. Recordings with $R_s > 30$ M Ω were excluded from statistical analysis. All recordings were acquired using a Multiclamp 700B amplifier and signals were low-pass filtered at 3 kHz and digitized at 10 kHz (DigiData 1550, Molecular Devices). The physiological data were analyzed using Clampfit 10 software (Molecular Devices) and Mini Analysis Program (Synaptosoft).

Western immunoblots

For Western immunoblots, NAc samples from retro-AAV-shRNA-DAT and retro-AAV-shRNA-Scramble injected mice were analyzed. The tissues were dissected in cold PBS, snap frozen in liquid nitrogen, and then lysed in lysis buffer (1% CHAPS, 137 mM NaCl, 2.7 mM KCl, 4.3 mM Na₂HPO₄, 1.4 mM KH₂PO₄, pH 7.2, 5 mM EDTA, 5 mM EGTA, 1 mM PMSF, 50 mM NaF, 1 mM Na₃VO₄, and protease inhibitors) at 4°C for 30 min. Lysates were centrifuged at 4°C to remove the insoluble deposit, run on 8% poly-acrylamide gels, and then transferred to nitrocellulose membranes.

Membranes were blocked for 2 h in TBST (150 mM NaCl, 10 mM Tris, 0.1% Tween 20, pH 7.6) containing 10% BSA. The primary antibody DAT (Alomone labs, catalog #AMT-003) was diluted in blocking buffer and incubated over-night at 4°C. After washing in PBS, the blots were incubated with HRP-conjugated secondary antibodies for 1 h at room temperature. After three washes, the blots were exposed to enhanced chemiluminescence substrate. Quantifications were performed by analyzing relative densities of exposed film using ImageJ.

Behavioral assays

Behavioral assays were performed when mice were 8–12 weeks old. All behavioral tasks were performed during the switching period of the light phase and the dark phase (18:00–20:00). Mice were placed in the room 3 h before tasks to adapt to the experimental environment. Behavioral tasks were performed 4h, 6h, 12h, 24h, or 3 days after propofol administration. For behavioral tasks with intra-NAc injection, intra-NAc injections of SCH23390 and PTX were performed 30 min before propofol administration.

Chronic restraint stress (CRS) was performed as previously described⁴⁷ Mice were subjected to CRS by putting them into 50 ml conical tubes during the light phase. Holes were drilled on the tubes to enable mice to breathe freely. The restraint persisted for 2–3 h per day for 16 consecutive days, as we found that 16 days of restraint induced more stable depressive-like and anhedonia-like behaviors than a 14-day protocol does.³⁸

For the sucrose preference test (SPT), mice were singly housed and adapted to one bottle of water and another bottle of 2% sucrose solution for 3 days. Then, mice were deprived of water for 24 h and then exposed to one bottle of 2 % sucrose solution and one bottle of water for 2 h. Bottle positions were switched after 1 h. The sucrose preference ratio was calculated by dividing the consumption of sucrose by the total consumption of both water and sucrose.⁴⁸

For the forced swimming test (FST), mice were individually put into a cylinder (15 cm diameter, 25 cm height) of water (27 °C) and allowed to swim for 6 min in the animal behavior test system (Shanghai Jiliang software technology Co., Ltd). Mouse behaviors were videotaped using a camera to the side of the swim cylinders. The immobility duration in the last 4 min of the test was measured by another member of our group who was blinded to mouse treatments. Immobility duration was defined to be the time when the mouse kept floating or motionless with only movements necessary for maintaining balance in the water.⁴⁹ Mice underwent a pre-experiment after the CRS procedure, in which the mice were placed in the cylinder under identical condition for 10 min to exclude mice that could not swim.

For the tail suspension test (TST), mice were suspended by binding their tail with adhesive tape fastened to a rail 50 cm from the ground. The height was high enough to ensure that the mice could not make other contact or climb during the test. A 6-minute video recording started immediately after the mice were taped. The immobility duration in the last 4 min of the experiment was measured by another member of our group who was blinded to mouse treatment.⁵⁰

For the open field test (OPT), the open field chamber was made of transparent plastic (50 cm \times 50 cm) and a 25 cm \times 25 cm center square was auto-defined by the behavioral software. Individual mice were placed in the center of the chamber and their behavior was monitored for 5 min. The time mice spent in the center area, the total distance they traveled and their velocity were monitored throughout the experiment.

For the elevated plus maze (EPM) test, the maze apparatus consisted of two opposing open (35 cm \times 6 cm) and two enclosed arms (35 cm \times 6 cm) extending from a central platform (6 cm \times 6 cm). The apparatus was raised 74 cm above the floor. During the test, mice were placed in the center square of the maze, facing an open arm, followed by a 5 min monitoring of their behavior. The entries into the open arms and the time they spent in the open arms were analyzed throughout the experiment. The apparatus was cleaned with 75% ethanol after each trial.

For conditioned place preference (CPP), a three-chamber apparatus was used. Two chambers (20*20*50cm) were distinguished by different wall colors (black and striated white) and floor patterns (spoke type and gridding) and separated by a corridor. A video tracking system was used to record mouse movements. Mice were handled and adapted to the environment for 3 days. On day 0, mice freely explored the apparatus for 15 min to record time spent in the chambers, and mice that spent over 70% of the time in either side were excluded. The conditioning session was conducted from day 1 to 7, with the black chamber associated with intraperitoneal injection of propofol at 100mg/kg for 45min, then 4 h later, the white chamber was associated with saline injections of the same volume for 45min. On the day 8, mice were allowed to freely explore the whole apparatus for 15 min to record time spent in the chambers. The CPP ratio was defined as time spent in the black chamber divided by time spent in both chambers.⁵¹

QUANTIFICATION AND STATISTICAL ANALYSIS

No statistical methods were used to pre-determine sample sizes, but our sample sizes are similar to those in previous reports^{52–54} and are typical of the field. Data distribution was assumed to be normal, but this was not formally tested. All statistical analyses were performed in GraphPad Prism 8.0 or MATLAB R2021a programs. All summary data are presented as the mean \pm SEM, superimposed with individual data. The sample size and statistical test for each experiment are indicated in the corresponding figure legend.